Volume 15 Issue 4 April 2007 ISSN 0967-0661

CONTROL ENGINEERING PRACTICE

A Journal of IFAC the International Federation of Automatic Control

CONTENTS

Continued on back cover

Available online at
ScienceDirect
www.sciencedirect.com

Available online at www.sciencedirect.com
ScienceDirect
Control Engineering Practice 15 (2007) 501–509
CONTROL ENGINEERING PRACTICE
www.elsevier.com/locate/conengprac

Modelling and model validation of heavy-haul trains equipped with electronically controlled pneumatic brake systems

M. Chou[a], X. Xia[a,*], C. Kayser[b]

[a]Department of Electrical, Electronic and Computer Engineering, University of Pretoria, Pretoria 0002, South Africa
[b]Spoornet Technology Management, Private Bag X637, Pretoria 0001, South Africa

Received 3 August 2005; accepted 11 September 2006
Available online 27 October 2006

Abstract

In this paper, a longitudinal dynamical model is proposed for heavy-haul trains equipped with electronically controlled pneumatic brake systems. It is validated against experimental data collected on a train with 200 wagons operated by Spoornet on its COALlink. Various data sets from actual trial runs, handwritten and electronic, off-line and on-line, are gathered and reconciled into a validation data set. Most system parameters are set in accordance with the experimental train setup, while certain parameters, such as damping coefficients, are estimated. The model is subjected to recorded input data for particular track sections. The resultant simulation outputs are compared to real-life data. From this study one may conclude that the longitudinal model is a justified choice for considering factors such as speed regulation, in-train force handling and energy consumption management of heavy-haul trains equipped with electronically controlled pneumatic brake systems.

Keywords: Electronically controlled pneumatic brake system (ECP); Heavy-haul train; Longitudinal dynamics; Model validation; Train modelling

1. Introduction

Mathematical modelling is an integral part of controller design. This process is subject to many different approaches, depending on the amount of available information and the desired objectives of the controller. Often, one should take care when striking a balance between model complexity and objective realisability. With sufficient information and understanding of the physical plant, mathematical equations can be used to describe the inner working of the plant in question.

The modelling of train dynamics can be very complex. A full set of 84 differential equations are needed in order to describe a conventional seven-body train wagon (Goodall & Kortum, 2002). Although certain degrees of freedom can sometimes be neglected, sufficient detailed descriptions of the motion dynamics are necessary to ensure stability, curving performance and ride quality (Garg & Dukkipati, 1984). This is especially true and under current active investigation in "mechatronic" trains with actively controlled suspension systems (Goodall & Kortum, 2002; Mei, Nagy, Goodall, & Wickens, 2002; Pearson, Goodall, Mei, & Himmelstein, 2004; Perez, Busturia, & Goodall, 2002).

Models with this type of complexity are, however, unnecessary for the handling of heavy-haul trains.

In train operations, the vehicle travels along the track. By considering only longitudinal operation, the degrees of freedom and the model complexity are reduced. On the other hand, track conditions are easy to obtain, as track gradient and curvature can be referred from the Geographical Information System (GIS). The key operation variables are the traction and braking forces the train driver applies. In this study, equations of motion are used to describe the longitudinal behaviour of long heavy-haul trains. This is a simplification of the full dynamical train model. It is also the purpose of this paper to justify the use of such a model to describe excessively long heavy-haul trains by validating it against real data collected during experimental trial runs.

On this operational level, existing general train models extend from the single-mass model, proposed by Howlett,

*Corresponding author. Tel.: +27 12 420 2165; fax: +27 12 362 5000.
E-mail address: xxia@postino.up.ac.za (X. Xia).

0967-0661/$ - see front matter © 2006 Elsevier Ltd. All rights reserved.
doi:10.1016/j.conengprac.2006.09.006

Milroy, and Pudney (1994) and Khmelnitsky (2000), to the spring-mass model proposed by Gruber and Bayoumi (1982) and Yang and Sun (2001). In particular, Astolfi and Menini (2002) explored the decoupling property of the model proposed by Yang and Sun (2001).

Note that most of these models are for passenger trains. General train models for heavy-haul trains equipped with the electronically controlled pneumatic brake system are scarce. None of the existing models, for both passenger and heavy-haul trains, has been validated against actual data.

In this study, a longitudinal train model for heavy-haul trains is proposed. It is validated against actual data from the COALlink trains operated by Spoornet in South Africa. By successfully validating the model, one provides evidence for the accuracy of the model. In addition, it provides a firm basis for controller design (see the companion paper Chou & Xia, 2006).

This paper is subdivided into three main topics: modelling methods, the validation process and the results from validation.

2. Modelling methods

2.1. ECP system

Pneumatic brakes are used in heavy-haul trains. For years, the control mechanism has been pneumatic-based. In this setup, a single brake pipe is connected through from the first locomotive to the last wagon, stretching over 2.5 km in the case of a 200-wagon COALlink train. Each wagon has its own equalising reservoir. The brake control valve at each wagon compares the brake pipe pressure to the reservoir pressure. Brake is applied when a drop in brake pipe pressure is detected. Excess air from the reservoir is diverted by the brake control valve into the brake cylinder, which applies the brake via the brake blocks, until the two pressures are once again equal.

Because of its pneumatic nature, the pressure drop propagates at a speed that is slightly less than the speed of sound, around 280 m s^{-1}. For a 200-wagon train stretching over 2.5 km, the signal delay is around 8–10 s. Adding the actuator delay, 100% brake application typically requires 3 min. Once the brake has been applied, consecutive brake application is limited by the remaining pressure in the equalising reservoir. A full reservoir recharge from a full service brake application could take as much as 15 min.

This dynamic nature adds substantial complexity to brake modelling. A simpler method is to ignore these behaviours. In the optimal scheduling posed by Howlett (1996), a diesel-powered passenger train was modelled as a single body mass. Since passenger trains are much shorter than heavy-haul trains, typically 15 carriages versus 200 wagons, this assumption is no longer justifiable for heavy-haul trains.

To model a train as a spring-mass system, as was done in Gruber and Bayoumi (1982) and Yang and Sun (2001), is not applicable to heavy-haul trains with the normal pneumatic brake system, owing to these brake delays.

The Electronic Controller Pneumatic (ECP) brake system, described by Kull (2001), AAR (2002) and Hawthorne (2003), replaces pneumatic control with electronic signals, while still utilising the same pneumatic braking mechanism. The brake pipe is now used solely for charging the reservoirs. Hundred percent brake application time is reduced to around 10 s (Spoornet, 2002). Because electronic signals are used to command the braking system, instantaneous braking across the whole train is now possible. In addition, variable brake application is also possible, as it is no longer constrained to the few brake application choices limited by the pneumatic signal.

These advancements allow the brake system to be modelled linearly, with limits on the maximum value and slew rate, as will be done in this study.

In locomotives, in addition to pneumatic braking, regenerative or rheostatic braking is also available. This is the preferred brake used by drivers because of its ability to dissipate large amount of energy. In COALlink trains, a wheel can dissipate up to 60 kW of energy, i.e., converting kinetic energy into heat energy. For a three-axle locomotive, this equals 360 kW. In comparison, the rheostatic brake of the 7E1 locomotive can dissipate up to 3000 kW through its resistor banks.

Because motors are used for energy conversion, rheostatic brake behaviour is dependent on the characteristic of the motor. Typical brake efforts at various notches are shown in the bottom graph in Fig. 1.

In the proposed longitudinal dynamics model, braking inputs are in terms of forces. A look-up table is used in this study to determine the available brake effort in relation to the current brake notch and speed of the train. This is to keep the accuracy of the notch-braking relationship of the deployed locomotives.

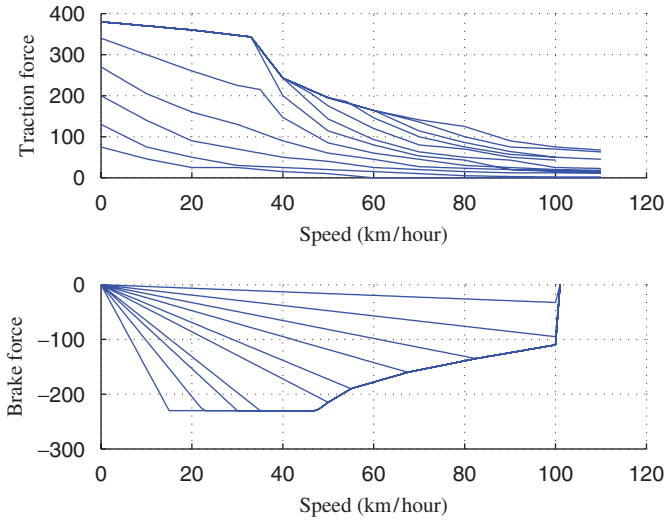

Fig. 1. Traction and brake efforts at different notches versus speed graph for 7E1 locomotive.

2.2. Traction

The traction behaviour of a locomotive depends on the type of motor used. In addition, it could be powered electrically or by diesel. For COALlink trains, AC electric locomotives are used. The traction efforts of the 7E1 locomotive at various notches are shown in Fig. 1.

A look-up table is again used in this study to determine the traction effort available under the current speed of the train and the traction notch level. The locomotive traction forces are constantly updated. This ensures the accuracy of the traction force at constantly varying speed.

It is due to these features after the introduction of the ECP system that spring-mass modelling becomes plausible for excessively long heavy-haul trains.

2.3. Coupler

With the traction and brake forces of each unit (wagon or locomotive) modelled, the next step is to link these individual units, or cars, together.

In COALlink trains, couplers and draw bars are used for linkage. Couplers are knuckle-like connectors with slack while draw bars are solid bars without slack. At the two ends of each car, draft gears connect to the undercarriage. Draft gears act as buffers and are connected to the coupler or draw bar. A complete linkage is shown in Fig. 2.

As the draft gears experience compression forces from the couplers, their overall lengths change up to the maximum displacement. A draft gear consists of rigid supporting frames as well as cushioning devices that provide damping. Once the draft gear travel reaches the maximum, the draft gear becomes solid and the impact forces are directly transmitted to the car body.

The draft gear, together with the coupler or draw gear, forms the coupler system, shown in Fig. 2. The knuckle-like coupler slack results in a dead band in the force displacement response. Below the maximum displacement the behaviour of the draft is elastic-like. The force displacement response of the coupler system is shown in Fig. 3.

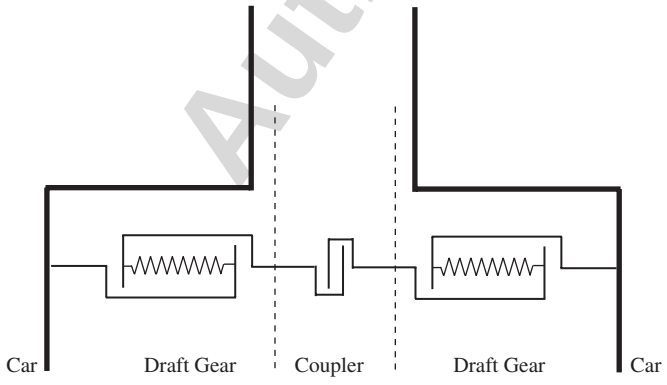

Fig. 2. Linkage system consisting of a coupler and draft gears.

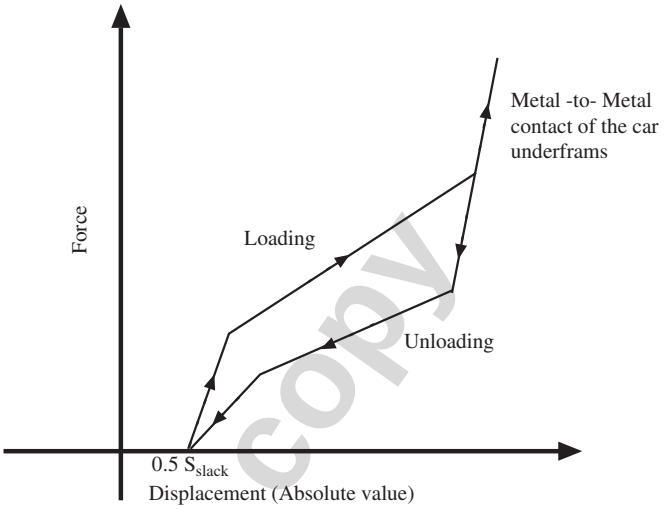

Fig. 3. Force displacement characteristic of the coupler system.

To simplify the calculations of over a hundred of coupler systems found in a heavy-haul train, the coupler system is taken as a spring with damping,

$$F_{coupler} = k_i(x_i - x_{i+1}) + d_i(\dot{x}_i - \dot{x}_{i+1}), \quad (1)$$

where k_i (the gradient of the curve in Fig. 3) and d_i are the spring and damping constants, and x_i, x_{i+1} and $\dot{x}_i$, $\dot{x}_{i+1}$ are the displacements and speed of the ith and $(i+1)$th wagons, respectively.

This approximation holds well when the draft gear travel is less than the maximum. Once it reaches the maximum, the coupler force becomes internal forces, which results in non-linearity.

In this study, the hard displacement limiters restrain the displacement within the limits at every sampling point. The spring constant of the coupler k_i varies individually between the normal and the maximum value, depending on its displacement values, approximating non-linearity.

The impact forces resulting from draft gears reaching their maximum displacement are not directly modelled in this paper.

2.4. Force model

Equations of motion are considered for each car individually, which is interconnected with the rest of the train via couplers. In practice, certain train configurations couple four wagons via rigid bars instead of couplers into a group called a rake. These rakes are then connected via couplers. In this study, these rakes are considered as a single entity with four times the mass and length of a wagon.

The two major resistances experienced by a train are rolling resistance and aerodynamic drag. While the former is experienced by each car, aerodynamic drag is experienced by the leading cars. In this paper, aerodynamic drag is only considered for the first car, often the locomotive, for

the sake of simplicity. The general resistance is given as

$$R = \underbrace{c_0 + c_v v}_{R^r} + \underbrace{c_a v^2}_{R^a}, \tag{2}$$

where v is the velocity of the car, R^r is the rolling resistance, R^a is the aerodynamic drag and the coefficients c_0, c_v, c_a are obtained experimentally.

Aerodynamic drag only becomes dominant during high speed operations. Therefore at the low speed at which heavy-haul trains operate, rolling resistance is the more significant factor.

The complete modelling is illustrated in Fig. 4. Simplified versions of the model were used in the passenger train study of Yang and Sun (2001) and Gruber and Bayoumi (1982).

In Fig. 4, n is the number of units, *i.e.*, rakes and locomotives. The equations of motion of the train are

$$\begin{aligned} m_1\ddot{x}_1 &= u_1 - k_1(x_1 - x_2) - d_1(\dot{x}_1 - \dot{x}_2) \\ &\quad - (c_0 + c_v\dot{x}_1)m_1 - c_a\dot{x}_1^2\left(\sum_{i=1}^{n} m_i\right) \\ &\quad - 9.98\sin\theta_1 m_1 - 0.004D_1 m_1, \end{aligned}$$

$$\begin{aligned} m_i\ddot{x}_i &= u_i - k_i(x_i - x_{i+1}) - k_{i-1}(x_i - x_{i-1}) \\ &\quad - d_i(\dot{x}_i - \dot{x}_{i+1}) - d_{i-1}(\dot{x}_i - \dot{x}_{i-1}) \\ &\quad - (c_0 + c_v\dot{x}_i)m_i - 9.98\sin\theta_i m_i \\ &\quad - 0.004D_i m_i, \quad i = 2, \ldots, n-1, \end{aligned}$$

$$\begin{aligned} m_n\ddot{x}_n &= u_n - k_{n-1}(x_n - x_{n-1}) \\ &\quad - d_{n-1}(\dot{x}_n - \dot{x}_{n-1}) - (c_0 + c_v\dot{x}_n)m_n \\ &\quad - 9.98\sin\theta_n m_n - 0.004D_n m_n, \end{aligned} \tag{3}$$

where $\dot{x}_i$ and x_i are the velocity and the displacement of the ith unit (locomotive or rake); k_i and d_i are the spring and damping constants of the coupler system; m_i and u_i are the mass and traction force of the ith unit, respectively; θ_i is the slope angle, while degree of curvature is calculated as $D_i = 0.5d_{wheelbase}/R$, R is the curve radius, as shown in Fig. 5 (Garg & Dukkipati, 1984). The gravitational and curvature resistance forces experienced by the car are $9.98m_i\sin(\theta_i)$ and $0.004m_iD_i$, respectively (Garg & Dukkipati, 1984).

Note that $u_i \leqslant 0$ if the ith unit is a rake. This is due to the fact that although the wagons are not powered in a heavy-haul train, they are still able to exert a braking force.

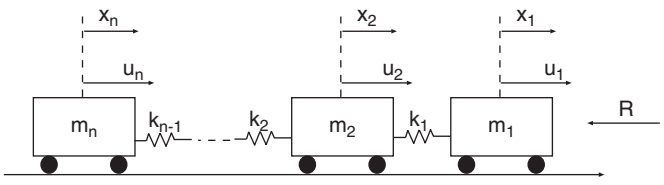

Fig. 4. Force diagram of the train.

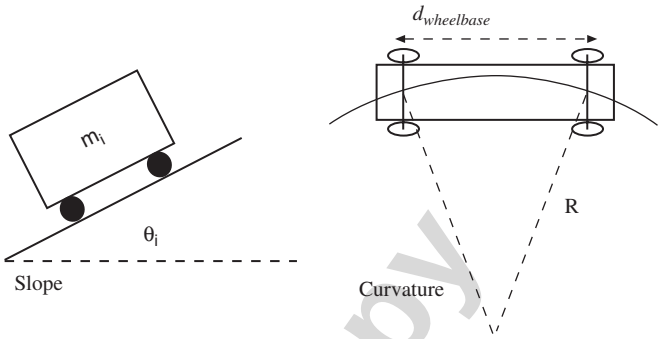

Fig. 5. Slope and curve angles.

3. Validation process

3.1. Setup

Three trial runs on the COALlink line were conducted on the 11th, 18th and 24th November 2003. All three trials completed the journey from the Ermelo depot to Richard's Bay harbour, but only certain sections were used in the simulations. Identical locomotives and wagon types were used. Couplers are of the same type within locomotive and wagon groups. These ECP equipped trains had different configurations as follows (from the front to the rear of the train):

- on the 11th: 4 locomotives—200 wagons—2 locomotives,
- on the 18th: 4 locomotives—100 wagons—2 locomotives—100 wagons, and
- on the 24th: 6 locomotives—200 wagons.

The simulation parameters are set to be the same as the trial runs. Worst-case values are assumed for the unavailable parameters. For example, smaller coupler damping coefficients, which produced more jittering, were used instead of larger values that produced a smoother response. The parameters from Table 1 are used. A section of the track where the train velocity is maintained with zero in-train force is chosen as the initial position for simulation. For example, for the trial run on the 11th November 2003, the initial position is chosen at the 12 km point from the start of the trial run at the Ermelo depot.

On the 18th November 2003, one of the front locomotives was faulty for a section of the track. This is simulated by setting its tractive and braking forces to zero, while still considering its mass. From the given record, this faulty locomotive was replaced after 64 km.

3.2. Data type

Four sets of data are available: GPS track data, GIS track data, handwritten input data and electronically recorded output data. GPS data contain longitudinal

Table 1
Heavy-haul train parameters

Parameter	Value	Unit
Locomotive		
Mass (7E1)	126 000	kg
c_0	7.6658×10^{-3}	$N\,kg^{-1}$
c_v	1.08×10^{-4}	$N\,s(m\,kg)^{-1}$
c_a	2.06×10^{-5}	$N\,s^2(m^2\,kg)^{-1}$
k	$78\sim121 \times 10^6$	$N\,m^{-1}$
d	$78\sim121 \times 10^4$	$N\,s\,m^{-1}$
Length	20.47	m
Max coupler slack	39.87×10^{-3}	m
Max traction	380	kN
Max brake	230	kN
Wagon		
Loaded mass	101 090	kg
c_0	6.3625×10^{-3}	$N\,kg^{-1}$
c_v	1.08×10^{-4}	$N\,s(m\,kg)^{-1}$
c_a	1.4918×10^{-5}	$N\,s^2(m^2\,kg)^{-1}$
k	$29.29\sim49 \times 10^6$	$N\,m^{-1}$
d	$29.29\sim49 \times 10^4$	$kg\,s^{-1}$
Length	12.07	m
Max coupler slack	77.5×10^{-3}	m
Max brake	100	kN
Wheelbase dist.	8.310	m
Simulation		
No. of wagons	200	
No. of locomotives	6	
Simulation time	2000	s
Sampling time	0.1–10	s
Input offset	−1.5	km

Table 2
Sample of the GPS data for COALlink line

Kilometre points	Longitude	Latitude	Altitude
0.178	−26.572	30.021	5586.014
0.176	−26.572	30.021	5585.942
0.174	−26.572	30.021	5585.871
0.172	−26.572	30.021	5585.799

and latitudinal coordinates and track altitude measured by an onboard barometer from a separate trial run, as shown in Table 2. Note that the height measurements contain many errors due to disturbance. GIS data contain track curvature and grade information, shown in Table 3. The GIS data are accurate. For this reason, the GIS data are used in the model simulation, the GPS data are only used to provide the initial altitude for the current track.

Table 4 contains train control inputs (notch settings) and the running speed of the train from the trial runs. These are handwritten. The train speed and in-train force outputs are electronically recorded, with some samples shown in Table 5.

Table 3
Sample of the GIS data for COALlink line

Kilometre points	Magnitude of feature	Type of feature
84.893	−1917	1
85.15	KMP 120	8
85.226	1600	3
85.45	Neutral section	8
85.555	−406	1

The types of feature are given as: 1, beginning of slope (distance per metre vertical); 2, beginning of curve (curve radius given in column 2 in m); 3, end of curve; 4, beginning of stop test (initial speed given in column 2 in $km\,h^{-1}$); 5, end of stop test; 8, name of the location.

Table 4
Samples of the handwritten input data

Kilometre points	moss pole	Trac 1 (notch)	Trac 2 (notch)	Brake	Current speed
6	1	14	0	0	64
8	1	0	0	0	52
10	1			STOP	
12	1	−1	6	0	38

3.3. Data reconciliation

3.3.1. Kilometre point offset

The handwritten control inputs are imprecise and sparse. The kilometre points for the handwritten notes are read off by the train technician from the kilometre signs as the train travels along the track. Eight to 24 signs are placed between kilometre points, with no indication as to how many have been placed for the current section. Furthermore, the kilometre signs are not strictly 1 km apart for logistic reasons. This results in offset errors in the kilometre information in the input data. Fig. 6 shows this situation for the data collected on the 11th November 2003; the offset between input and output kilometre points can be clearly seen in the second graph.

The electronically recorded outputs are very precise. The input and output data are reconciled via the common speed information found in both data sets. This compensates for the kilometre points offset between the two.

For the validation process, the reconciled inputs are fed into the model. The resultant in-train force and velocity are compared with the recorded results.

3.4. Input/output data offset

Because of the imprecise nature of kilometre signs as well as the human factor, sometimes there are offsets in the kilometre points of the recorded control signals.

In all validation simulation runs, the control signals are assumed to be accurate. In some cases, the simulated results show very large deviations from the corresponding electronically recorded outputs. An example is in Fig. 7.

Table 5
Samples of the output data for COALlink line during a trial run

Date	Time	Distance (km)	Speed (km h^{-1})	Coupler A load (kN)	Brake pipe (kPa)
2003/11/24	17:0:37.14	26.777054E − 3	0.000	268.945312	536.000977
2003/11/24	17:0:38.13	26.777054E − 3	0.000	268.872070	535.986328
2003/11/24	17:0:39.12	26.777054E − 3	0.000	268.395996	536.147461
2003/11/24	17:0:40.11	26.777054E − 3	0.000	268.615723	536.030273

Date	Time	Distance (km)	Brake cylinder (kPa)	Wagon 1 bar (kN)
2003/11/24	17:0:37.14	26.777054E − 3	0.029297	323.876953
2003/11/24	17:0:38.13	26.777054E − 3	0.073242	324.267578
2003/11/24	17:0:39.12	26.777054E − 3	0.058594	323.144531
2003/11/24	17:0:40.11	26.777054E − 3	−0.102539	323.828125

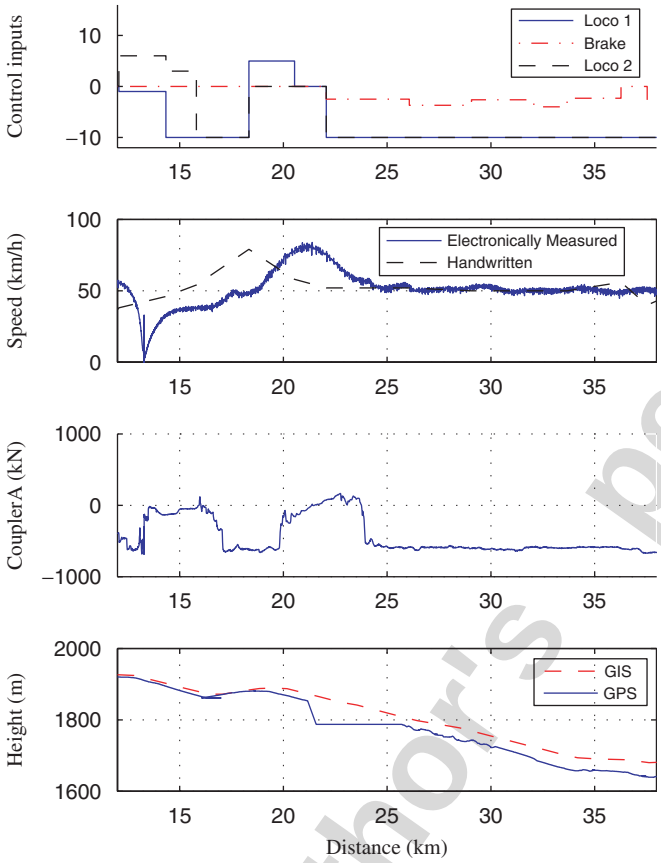

Fig. 6. Validated result with input compensation.

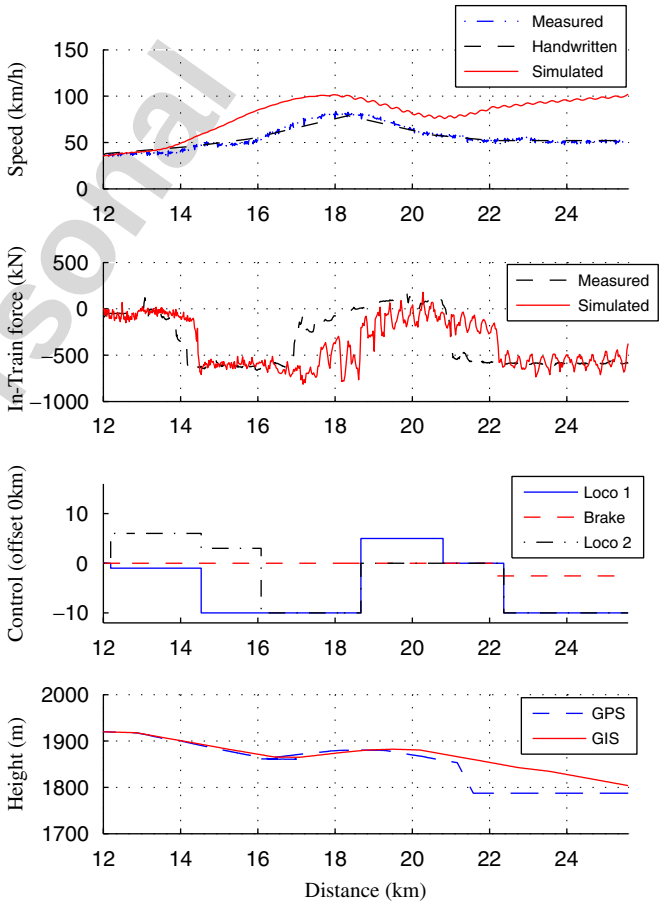

Fig. 7. Original simulated result using recorded input control signals directly.

Examining its velocity and in-train forces graphs shows an offset between the recorded in-train forces and the hand-written control signals. Since changes in traction and braking are the main cause for in-train force variations, any variations of two data should correspond. After examining other data, this has proven to be true.

The control signal in Fig. 7 lags behind the recorded in-train forces by 1.5 km. Examining the other sections of that particular run reveals that the offset is approximately constant.

By only compensating for these control signal offsets, the results are significantly improved, as shown in Fig. 8. The velocity and in-train force simulated outputs now correspond very closely to the recorded values.

3.5. Sampling time

Sampling time determines the number of simulation steps required for the given simulation time. A smaller

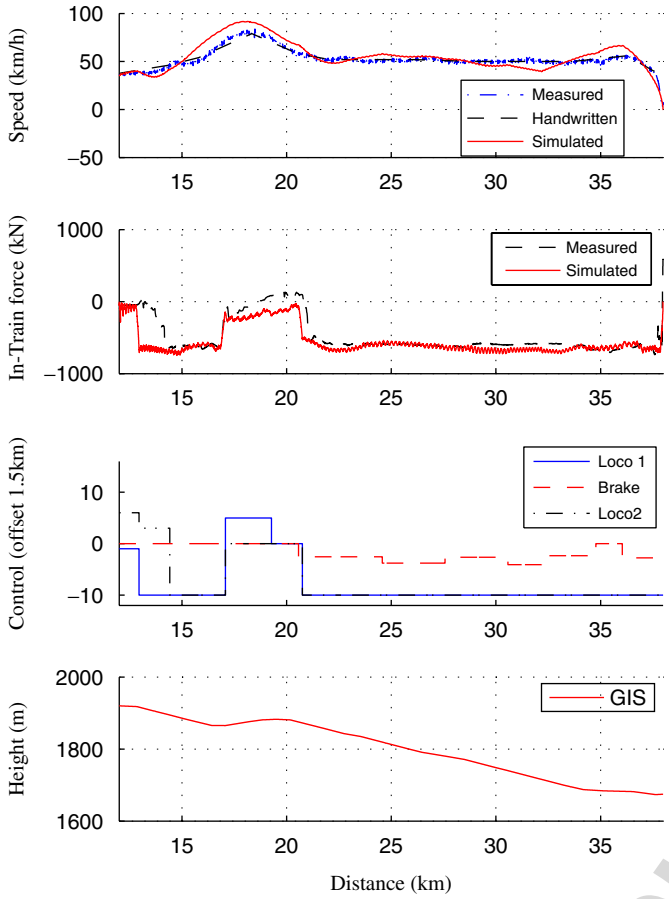

Fig. 8. Control signal offset compensated simulated result.

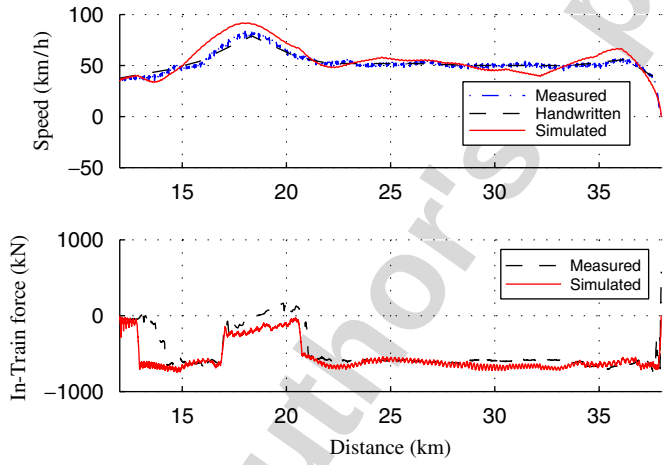

Fig. 9. Simulated result with 0.1 s sampling time.

sampling time often results in improved accuracy, yet decreasing the sampling time by tenfold equals to tenfold the computational cycles. Thus it is necessary to find a balance between accuracy and computational cycles.

Data from the 18th November 2003 trial run are used for this simulation set. The simulation results in Fig. 9 show the velocity of the first locomotive and the in-train force of the front coupler of the first wagon, with a simulation

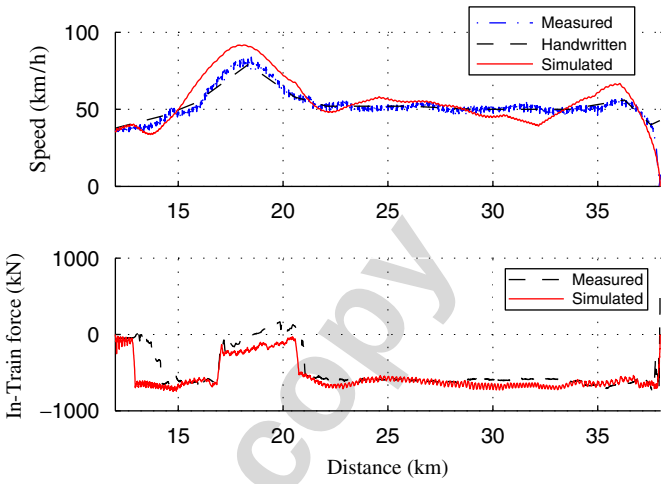

Fig. 10. Simulated result with 0.5 s sampling time.

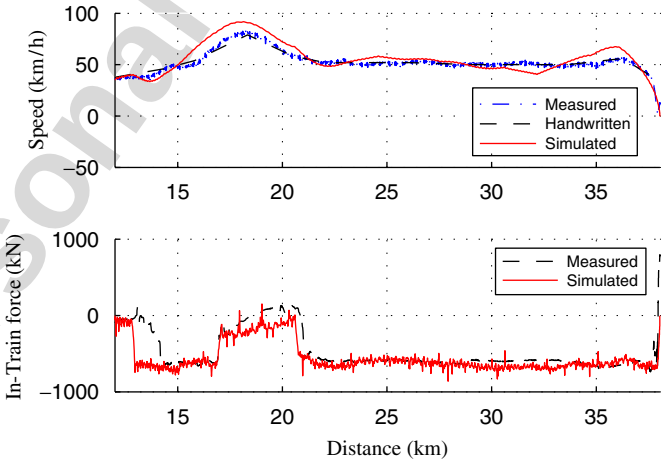

Fig. 11. Simulated result with 1 s sampling time.

sampling time t_s of 0.1 s. Figs. 10 and 11 show similar simulation outputs with t_s of 0.5 s and 1 s, respectively. Control inputs and track topology are exactly the same for all three simulation runs and are therefore not shown.

From the graphs, it is clear that as sampling time grows longer, the simulated in-train force output starts to show more jittering and small peaks that depart from the recorded outputs. Velocity tracking outputs do not seem to be affected by the sampling time changes. Thus, t_s of 1 s is too little to provide accurate results, while t_s of 0.5 s provides accuracy similar to t_s of 0.1 s at one-fifth of the computational cycles.

3.6. Damping coefficient

From the draft gears' data sheets, the spring coefficients can be determined from the force–displacement characteristic curves. However, the damping coefficients are not available. For the simulation, a fraction of the spring coefficient is used.

Fig. 12 compares the simulated velocity and in-train force outputs with zero damping coefficients. The damping

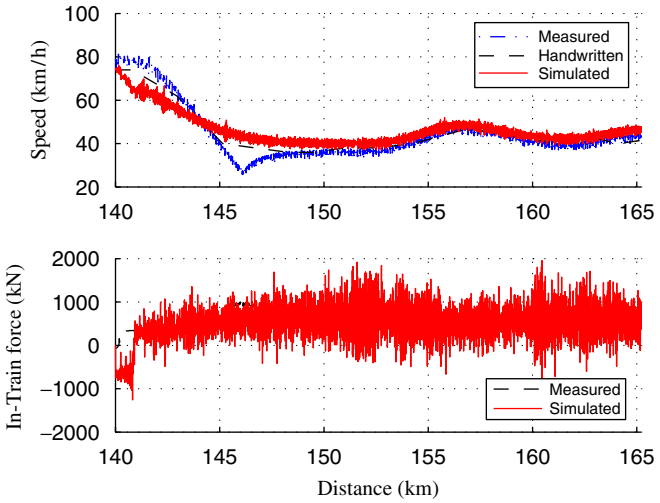

Fig. 12. Simulated result with zero damping coefficient.

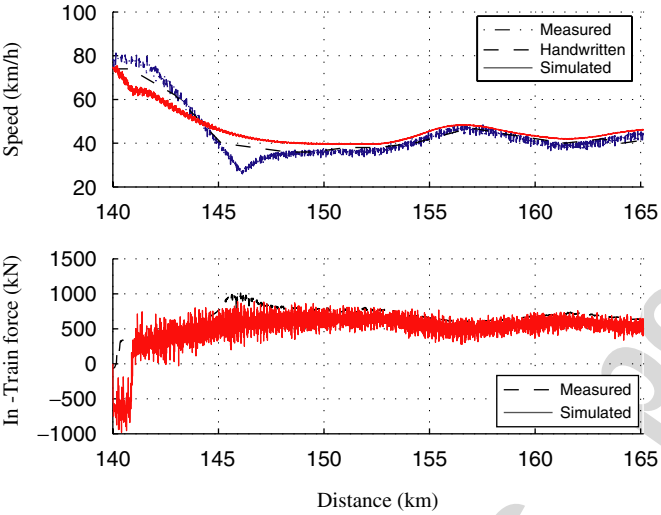

Fig. 13. Simulated result with damping coefficient of 0.0001 times the spring coefficient.

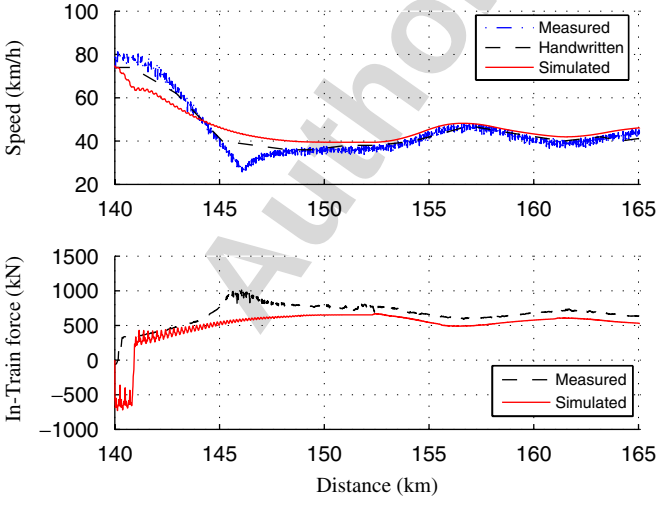

Fig. 14. Simulated result with damping coefficient of 0.01 times the spring coefficient.

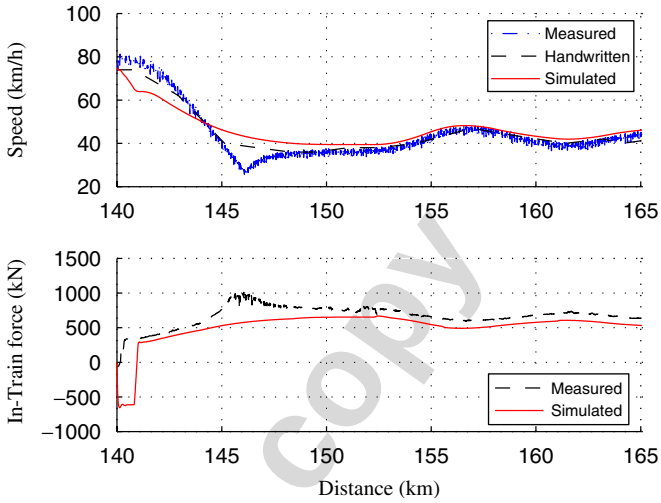

Fig. 15. Simulated result with damping coefficient equal to the spring coefficient.

coefficients are then increased progressively from $0.0001k_i$, $0.01k_i$ and finally k_i, with k_i being the spring coefficients. Similar figures of these results are shown in Figs. 13–15. Train setup and recorded data from the 11th November 2003 are used, when a different section of track was used.

From the simulation, it is very clear that in-train force is greatly influenced if the damping coefficients are set too small. With damping coefficients above $0.01k_i$, the simulation results correspond most closely to the recorded data, in terms of transient jittering and steady-state behaviour. This shows that there is some robustness of the damping coefficients in a reasonable range.

4. Conclusion

The simulated output shows that the model is able to produce similar behaviour as the actual train. The minor errors are due to imprecise parameters, such as wagon mass, weather and track conditions and unknown disturbances.

From the simulation, it is found that velocity output depends on both control inputs and track grade. In comparison, in-train forces are less influenced by track grade but tied more strongly to control input fluctuations. It may be possible that a well designed controller could eliminate most of the track grade-induced in-train forces. This translates to train handling improvement without resorting to other expensive options such as additional locomotives or individual braking.

Results show that simulation sampling time affects the accuracy of the train simulation. A trade-off between simulation computation time and accuracy has to be made. The fact that in-train forces are more sensitive to simulation sampling time variation shows that in-train force dynamics are fast in nature. Velocity change, in comparison, is a slow dynamic.

Results also show that the model has a certain robustness against damping coefficients when set in proper ranges.

The successful validation confirms that the proposed model for heavy-haul trains is able to simulate the longitudinal motion of the actual train. This provides a firm basis for future modelling refinements and controller designs. The accompanying paper (Chou & Xia, 2006) on optimal cruise control of heavy-haul trains equipped with ECP systems, utilises this validated model for controller design as well as a testing platform for controller performance.

References

AAR (2002). *Manual of standards and recommended practices, electronically controlled brake system*. Technical Report, Association of American Railroads.

Astolfi, A., & Menini, L. (2002). Input/output decoupling problems for high speed trains. In *Proceedings of the American control conference* (pp. 549–554).

Chou, M., & Xia, X. (2006). Optimal cruise control of heavy-haul trains equipped with electronically controlled pneumatic brake systems. *Control Engineering Practice*, in press, doi:10.1016/j.conengprac.2006.09.007.

Garg, V. K., & Dukkipati, R. V. (1984). *Dynamics of railway vehicle systems* (xiii ed.). Toronto: Academic Press.

Goodall, R. M., & Kortum, W. (2002). Mechatronic developments for railway vehicles of the future. *Control Engineering Practice*, *10*, 887–898.

Gruber, P., & Bayoumi, M. M. (1982). Suboptimal control strategies for multilocomotive powered trains. *IEEE Transaction on Automatic Control*, *27*(3), 536–546.

Hawthorne, M. J. (2003). Real world benefits from electronic train control technologies. *Heavy haul conference*, Dallas, May 2003.

Howlett, P. (1996). Optimal strategies for the control of a train. *Automatica*, *32*(4), 519–532.

Howlett, P. G., Milroy, I. P., & Pudney, P. J. (1994). Energy-efficient train control. *Control Engineering Practice*, *2*, 193–200.

Khmelnitsky, E. (2000). On an optimal control problem of train operation. *IEEE Transaction of Automatic Control*, *45*(7), 1257–1266.

Kull, R. C. (2001). Wabtec ECP system update. In *Proceedings of the 2001 IEEE/ASME joint railroad conference* (pp. 129–134).

Mei, T. X., Nagy, Z., Goodall, R. M., & Wickens, A. H. (2002). Mechatronic solutions for high-speed railway vehicles. *Control Engineering Practice*, *10*, 1023–1028.

Pearson, J. T., Goodall, R. M., Mei, T. X., & Himmelstein, G. (2004). Active stability control strategies for a high speed bogie. *Control Engineering Practice*, *12*, 1381–1391.

Perez, J., Busturia, J. M., & Goodall, R. M. (2002). Control strategies for active steering of bogie-based railway vehicles. *Control Engineering Practice*, *10*, 1005–1012.

Spoornet (2002). *Introduction to electronic control pneumatic brake and wire distributed power*. Technical Report, Spoornet.

Yang, C. D., & Sun, Y. P. (2001). Mixed H_2/H_∞ cruise controller design for high speed trains. *International Journal of Control*, *74*(9), 905–920.